JCTC Journal of Chemical Theory and Computation

Letter

pubs.acs.org/JCTC

Including Torsional Anharmonicity in Canonical and Microcanonical Reaction Path Calculations

Jingjing Zheng and Donald G. Truhlar*

Department of Chemistry, Chemical Theory Center, and Supercomputing Institute, University of Minnesota, Minneapolis, Minnesota 55455-0431, United States

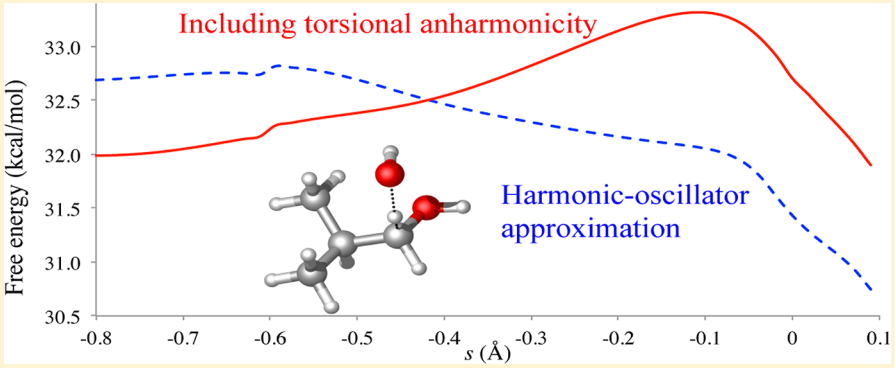

ABSTRACT: We reformulate multistructural variational transition state theory by removing the approximation of calculating torsional anharmonicity only at stationary points. The multistructural method with torsional anharmonicity is applied to calculate the reaction-path free energy of the hydrogen abstraction from the carbon-1 position in isobutanol by OH radical. The torsional potential anharmonicity along the reaction path is taken into account by a coupled torsional potential. The calculations show that it can be critical to include torsional anharmonicity in searching for canonical and microcanonical variational transition states. The harmonic-oscillator approximation fails to yield reasonable free energy curves along the reaction path.

This article is concerned with including torsional anharmonicity in rate constants calculated by variational transition state theory[1−4] (the readers is referred to reviews for additional references[5−8]) with a sequence of transition state dividing surfaces[4,9,10] that intersect a minimum-energy path.[11]

In both thermodynamics and kinetics, the harmonic-oscillator (HO) approximation is the most widely used approach for describing molecular vibrations. In our work, we scale the harmonic frequencies with scale factors[12] parametrized to yield (on average) accurate zero-point energies, and hence our calculations include anharmonicity. When we use scaled harmonic frequencies, we call the result quasiharmonic (QH). Although the QH approximation is often good enough (for the accuracy needed here) for calculating accurate zero-point energy because that is the scale factor we choose to use and because zero-point energies are dominated by high-frequency stretches that show systematic errors that can be approximately corrected by parametrization, the QH approximation can lead to significant errors for treating low-frequency vibrations, e.g., torsions. Recently, we developed a method called the multistructural method including torsional anharmonicity (MS-T)[13,14] that can efficiently and accurately treat low-frequency torsions, even when they are strongly coupled. This method has been applied to various complex molecules, radicals, and transition states to study their thermodynamics. On the basis of the MS-T method, multipath variational transition state theory (MP-VTST)[15,16] was developed for calculating thermal rate constants for reactions with multiple conformational structures of reactants, products, and transition states. When only one path is explicitly calculated to represent all paths in MP-VTST, we call it multistructural variational transition state theory (MS-VTST).[17] However, in work reported so far we used the QH approximation in reaction-path calculations for locating variational dividing surfaces by assuming that the multistructural anharmonicity at the variational transition state can be modeled by the anharmonicity at the conventional transition state. This approximation may be good enough when the variational transition state is close to the saddle point, but it clearly becomes questionable for the general case. In this letter, we present a case where the breakdown of the harmonic-oscillator approximation due to torsional anharmonicity leads to a large error in finding the variational transition state.

The multipath (MP) canonical variational theory (CVT) rate constant including multidimensional tunneling (MT) for a bimolecular reaction is[16]

Received: March 22, 2013

   dx.doi.org/10.1021/ct400231q | J. Chem. Theory Comput. XXXX, XXX, XXX−XXX

$$k^{\mathrm{MP-CVT/MT}} = \frac{k_B T}{h}\frac{Q^{\ddagger}_{\mathrm{elec}}}{\Phi^{\mathrm{MS\text{-}T,R}}}\exp(-\beta V^{\ddagger})\sum_{k=1}^{K}\kappa_k\Gamma_k^{\mathrm{CVT}}Q_k^{\mathrm{T},\ddagger} \approx \gamma\frac{k_B T}{h}\frac{Q^{\ddagger}_{\mathrm{elec}}\sum_{k=1}^{K}Q_k^{\mathrm{T},\ddagger}}{\Phi^{\mathrm{MS\text{-}T,R}}}\exp(-\beta V^{\ddagger}) \quad (1)$$

where γ is a generalized transmission coefficient specified below, K is the number of distinguishable conformational structures of the transition state, β is $1/k_B T$, k_B is Boltzmann's constant, T is temperature, h is Planck's constant, $Q^{\ddagger}_{\mathrm{elec}}$ is the electronic partition function of the conventional transition state (which is denoted as ‡), $\Phi^{\mathrm{MS\text{-}T,R}}$ is the bimolecular reactants' partition function per unit volume (with its zero of energy at the potential energy of the lowest-energy reactant structure), $Q_k^{\mathrm{T},\ddagger}$ is the rovibrational partition function of saddle point k with torsional potential anharmonicity (T), and $V^{\ddagger}$ is the classical barrier height (defined as the potential energy increase (if positive) or decrease (if negative) in changing from the zero of energy used for the reactant partition function to the zero of energy used for the transition state partition functions $Q_k^{\mathrm{T},\ddagger}$, which (for all k) is the saddle point energy of the lowest-energy conformational structure (k = 1) of the saddle point). The generalized transmission coefficient γ is approximated by

$$\gamma = \frac{\sum_{k=1}^{P}\kappa_k\Gamma_k^{\mathrm{CVT}}Q_k^{\mathrm{T},\ddagger}}{\sum_{k=1}^{P}Q_k^{\mathrm{T},\ddagger}} \quad (2)$$

where P is the number of distinguishable transition structures used to compute the tunneling transmission coefficient κ_k and the CVT recrossing transmission coefficient Γ_k^{CVT} (where $P \le K$). Note that the wavy equal sign in the second line of eq 1 can be replaced by a straight equal sign if P equals K.

Previously, we calculated Γ_k^{CVT} based on approximating the reaction-path dependence of the transition state partition function by the QH approximation, i.e.,

$$\Gamma_k^{\mathrm{CVT}}\ (\mathrm{previous}) = \frac{Q_k^{\mathrm{QH,CVT}}}{Q_k^{\mathrm{QH},\ddagger}} \quad (3)$$

where the numerator and denominator are respectively QH rovibrational partition functions for the canonical variational transition state along reaction path k and conventional transition structure k, from which it originates. A more accurate approximation, to be used for the first time in the present letter, is

$$\Gamma_k^{\mathrm{CVT}}\ (\mathrm{new}) = \frac{Q_k^{\mathrm{T,CVT}}}{Q_k^{\mathrm{T},\ddagger}} \quad (4)$$

where $Q_k^{\mathrm{T,CVT}}$ is the rovibrational partition function with multistructural torsional anharmonicity of the canonical variational transition state associated with saddle point k.

For a reaction with a large number of conformational structures of the transition state, it can be expensive to calculate all the reaction paths used in eq 2. An economical approximation is to base the tunneling transmission coefficient and variational effect on the lowest energy path (k = 1). This yields multistructural variational transition state theory:

$$k^{\mathrm{MS-CVT/MT}} = \kappa_1\Gamma_1^{\mathrm{CVT}}\frac{k_B T}{h}\frac{Q^{\ddagger}_{\mathrm{elec}}\sum_{k=1}^{K}Q_k^{\mathrm{T},\ddagger}}{\Phi^{\mathrm{MS\text{-}T,R}}}\exp(-\beta V^{\ddagger}) = \kappa_1\frac{k_B T}{hC^{\circ}}Y^{\mathrm{MS}}\exp\left[-\frac{1}{RT}\max\Delta G_1^{\mathrm{T,GT},\circ}(s)\right] \quad (5)$$

where

$$Y^{\mathrm{MS}} = \frac{\sum_{k=1}^{K}Q_k^{\mathrm{T},\ddagger}}{Q_1^{\mathrm{T},\ddagger}} \quad (6)$$

$$\Delta G_1^{\mathrm{T,GT},\circ} = -RT\ln\left[\frac{Q^{\ddagger}_{\mathrm{elec}}C^{\circ}}{\Phi^{\mathrm{MS\text{-}T,R}}}Q_1^{\mathrm{T,GT}}(s)\right] + V_{\mathrm{MEP}}(s) \quad (7)$$

and R is the gas constant, C° is the gas-phase concentration under standard-state conditions (in molecules per unit volume, and since standard states of gases are ideal, it equals $P^{\circ}/k_B T$, where P° = 1 bar), $\Delta G_1^{\mathrm{T,GT},\circ}(s)$ is the generalized-transition-state (GT) standard-state free energy of activation[18] as a function of the progress variable s along reaction path k = 1 (s is the signed distance from saddle point k = 1 in isoinertial coordinates scaled to 1 amu, and the subscript 1 denotes k = 1), and $V_{\mathrm{MEP}}(s)$ is the generalized-transition-state potential energy. The factor Y^{MS} is the rate increase (by definition, Y^{MS} is greater than or equal to unity) due to the multistructural anharmonicity of the transition state.

Next, we consider partition functions of reactants and transition structures. A conventional transition structure is the structure of a saddle point of the potential energy surface, i.e., the structure of the lowest-energy geometry of the conventional-transition-state dividing surface, just as an "equilibrium structure" is the structure of a local minimum of the potential energy surface. A generalized transition structure is a structure associated with a generalized transition state, which is any transition-state dividing surface or trial transition-state dividing surface, not just the conventional-transition-state dividing surface. Just as "transition state" is often used generically to refer to both conventional and generalized transition states, we will use "transition structure" to refer generically to both conventional and generalized transition structures. Note that partition functions of transition structures are missing one degree of freedom (the reaction coordinate). We use j = 1, ..., J to label stable structures and k = 1, ..., K to label transition structures; we write the next several formulas using j and J, but the formulas also apply to transition structures by changing j to k and J to K and by remembering that one degree of freedom is missing. The conformational-rovibrational partition function using the MS-T method for a species with J conformational structures is[14]

$$Q_{\mathrm{con\text{-}rovib}}^{\mathrm{MS\text{-}T}} = \sum_{j=1}^{J}Q_j^{\mathrm{T}} \quad (8)$$

$$Q_j^{\mathrm{T}} \equiv Q_{\mathrm{rot},j}\exp(-\beta U_j)Q_j^{\mathrm{QH}}T_j \quad (9)$$

where Q_j^{T} is the contribution of structure j to the rovibrational partition function with torsional anharmonicity, $Q_{\mathrm{rot},j}$ is the classical rotational partition function for structure j, U_j is its relative potential energy, Q_j^{QH} is its QH vibrational partition function partition function, and T_j is a factor to account torsional-potential anharmonicity for all torsional modes in the structure j. In particular, T_j is[14]

dx.doi.org/10.1021/ct400231q | J. Chem. Theory Comput. XXXX, XXX, XXX−XXX

$$T_j = (2\pi\hbar\beta)^{t/2} \frac{\prod_{m=1}^{F} \omega_{j,m}}{\prod_{\overline{m}=1}^{F-t} \overline{\omega}_{j,\overline{m}}} \frac{\sqrt{\det \mathbf{D}_j}}{\prod_{\tau=1}^{t} M_{j,\tau}} \prod_{\eta=1}^{t} \exp(-\beta W_{j,\eta}/2) I_0(\beta W_{j,\eta}/2) \quad (10)$$

where t is number of torsional modes, F is number of bound vibrational modes (stretches, bends, and torsions), $\omega_{j,m}$ and $\overline{\omega}_{j,\overline{m}}$ are respectively the normal-mode harmonic frequencies and the torsion-projected normal-mode frequencies (both sets are scaled), $\mathbf{D}_j$ is the moment of inertia matrix of Kilpatrick and Pitzer,[19] $W_{j,\eta}$ is the torsional barrier height based on a coupled torsional potential, and I_0 is a modified Bessel function. The details of the MS-T calculations can be found in ref 14. All MS-T calculations were performed by the *MSTor* program.[20−22]

The multistructural microcanonical variational transition state with a multidimensional tunneling (MS-μVT/MT) rate constant can be calculated by replacing $\Gamma_{k=1}^{\mathrm{CVT}}$ (new) in eq 1 by

$$\Gamma_k^{\mu\mathrm{VT}} = \frac{\beta \int_0^\infty \exp(-\beta E) N_k^{\mu\mathrm{VT}}(E)\, \mathrm{d}E}{Q_k^{\mathrm{T},\ddagger}} \quad (11)$$

$$N_k^{\mu\mathrm{VT}} = \min_s \{N_k(E, s)\} \quad (12)$$

where E is total rovibrational energy relative to the threshold energy, and $N_k^{\mu\mathrm{VT}}(E)$ is the microcanonically minimized sum of states for energy levels below E; $N_k^{\mu\mathrm{VT}}(E)$ is obtained by searching for the minimum of the sum of states $N_k(E,s)$ along the reaction coordinate s. In order to include torsional anharmonicity in $N_k(E,s)$, it is calculated from the inverse Laplace transform[23] of $Q_k^{\mathrm{T}}(T)$ along the reaction coordinate s.

Anharmonicity is known to be important for unimolecular microcanonical rate constants evaluated by RRKM theory.[24] In this letter, we show the importance of including torsional anharmonicity for locating the correct canonical and microcanonical variational transition states of a bimolecular reaction. The case studied in this letter is the hydrogen abstraction reaction from carbon-1 in isobutanol by an OH radical:

$$(CH_3)_2CHCH_2OH + OH \rightarrow (CH_3)_2CHCHOH + H_2O \quad (R1)$$

In the reaction path calculations, eq 8 is applied to the saddle point and nonstationary points along the reaction path (with $j \rightarrow k = 1$ in the latter case) to obtain free energy curves with torsional anharmonicity at various temperatures. Generalized normal-mode frequencies along the reaction path are calculated by using nonredundant internal coordinates[25,26] with the reaction coordinate projected out. For comparison purposes, we also present results for which the QH partition functions are used for the reaction path calculations. The potential energy surfaces are calculated by the density functional M08-HX[27] with the MG3S[28,29] basis set. Note that the MG3S basis set is equivalent to the 6-311+G(2df,2p) basis set for elements H, C, and O. The accuracy of the M08-HX/MG3S density functional is validated against the benchmark calculations by the CCSD(T)-F12a[30−32] method with the jun-cc-pVTZ[33] basis set. A factor of 0.973 is used to scale all the frequencies calculated by the M08-HX/MG3S method; the scaling is based on obtaining a more accurate zero point energy.[12]

We found 20 saddle points (10 pairs of mirror images) for this reaction and nine conformational structures for isobutanol. The zero-point-exclusive and zero-point-inclusive energies of these 10 pairs of saddle points relative to the infinitely separated lowest-energy structure of isobutanol and the OH radical are listed in Table 1. The reaction path and reaction path frequencies associated with the lowest-energy saddle point were calculated by direct dynamics using the *POLYRATE*[34] and *GAUSSRATE*[35] programs. The range calculated is [−0.85, 0.10] Å; the step size is 0.002 Å. A Hessian is calculated every nine steps.

Table 1. Zero-Point Exclusive and Inclusive Energies (in kcal/mol) of Saddle Points Relative to the Infinitely Separated Lowest-Energy Structure of Isobutanol and OH Radical

saddle point	V^a	$(V+\mathrm{ZPE})^b$
	M08-HX/MG3S	
1, 2	−0.45	−0.97
3, 4	−0.33	−0.90
5, 6	−0.12	−0.68
7, 8	−0.02	−0.46
9, 10	0.14	−0.39
11, 12	0.15	−0.65
13, 14	0.30	−0.29
15, 16	0.66	−0.05
17, 18	0.78	0.10
19, 20	1.10	0.25
	CCSD(T)-F12a/jun-cc-pVTZ[c]	
1, 2	−0.34	−0.86[d]

[a]Relative to the equilibrium potential energy of OH + isobutanol. The spin−orbit energy of 0.20 kcal/mol for the OH radical is included here and in generalized free energy of activation and rate constant calculations. Frequencies are scaled here, and Hessians are scaled in an equivalent way (i.e., by the square of 0.973) for all reaction-path and rate constant calculations. [b]Relative to ground-state energy (including ZPE) of OH + isobutanol. The spin−orbit energy of 0.20 kcal/mol for the OH radical is included. [c]Single-point energy at M08-HX/MG3 geometry. [d]CCSD(T)-F12a/jun-cc-pVTZ energies; scaled M08-HX/MG3S frequencies.

Figure 1 shows that the QH and torsional treatments of the generalized standard-state free energy of activation are quite different. At high temperatures, above ∼1000 K, the free energy profiles obtained by the QH approximation monotonically increase from the product side to the reactant side so that the canonical variational transition state cannot be located within the broad s range shown in Figure 1 because there is no maximum along the curves calculated by the QH approximation.

What causes the QH free energy curves to monotonically increase as s decreases? Are these free energy curves realistic? Changes of low frequencies usually have a significant impact on the partition function and free energy, especially at high temperature. Figure 2a shows the lowest frequency (a torsional mode) along the reaction coordinate. This frequency changes by up to a factor of 2.4 along the path. The large variation of the lowest frequency is the major reason for the free energy increasing monotonically from the product side to reactant side at high T. It is well-known that the harmonic-oscillator or QH approximation has large errors for the free energies of modes with frequencies below ∼100 cm^{-1}. By using the torsional anharmonicity correction in eq 8, quantum harmonic-oscillator partition functions and classical harmonic-oscillator partition functions for torsional modes are canceled at high temperatures so that all QH partition functions of torsional modes are replaced by the classical partition function based on a coupled torsional potential. Note that partition functions for a quantum harmonic oscillator and classical harmonic oscillator differ by less than 10%

dx.doi.org/10.1021/ct400231q | J. Chem. Theory Comput. XXXX, XXX, XXX−XXX

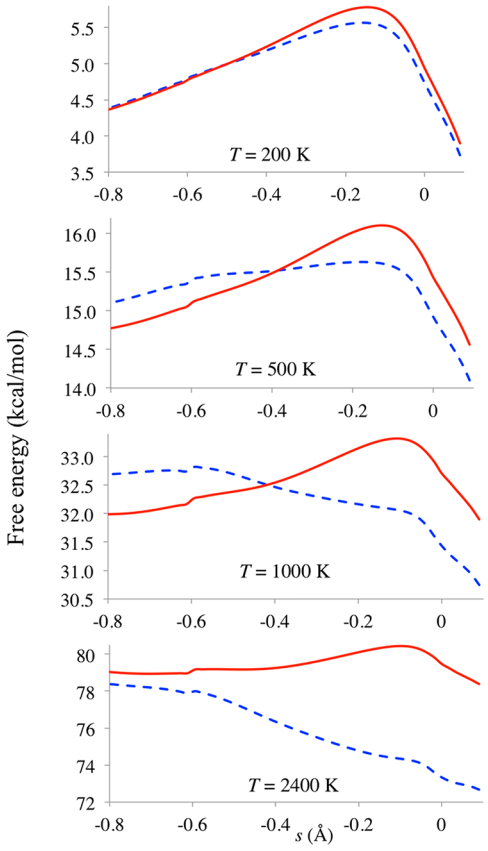

Figure 1. Standard-state generalized free energy of activation profile along the lowest-energy reaction path at various temperatures calculated by the QH approximation ($\Delta G_1^{QH,GT,o}$, blue dashed line) and by taking account of torsional anharmonicity using eq 9 ($\Delta G_1^{T,GT,o}$, red solid line).

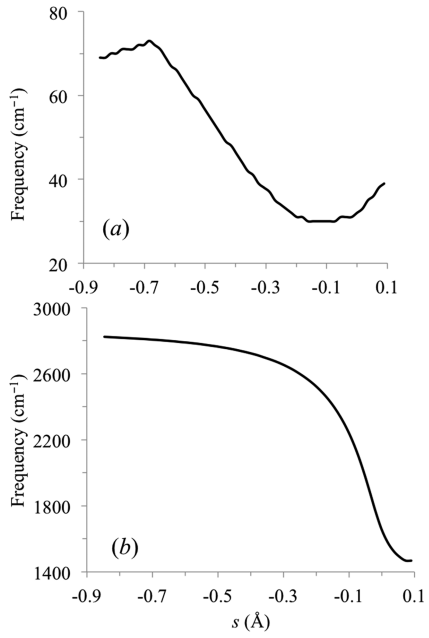

Figure 2. Harmonic frequencies along reaction path 1: (a) the lowest frequency and (b) the frequency that has the largest changes along the reaction path and that is primarily responsible for the variational effect.

for a frequency of 100 cm^{-1} above 100 K. The free energy curves calculated by including torsional anharmonicity have peaks close to the saddle point for temperatures up to 2400 K. These maxima on the free energy curves are the canonical variational transition states at the corresponding temperatures.

The generalized standard-state of activation profiles at various temperatures show that the maxima are not located at saddle point ($s = 0$), i.e., the best dynamical bottleneck is not a dividing surface passing through the saddle point. For example, the maximum at 200 K is located at $s = -0.15$ Å, where it is 0.84 kcal/mol higher than the standard-state of activation of the saddle point; this changes the calculated rate constant by a factor of 9 at 200 K. This large variational effect is caused by a significant change of one frequency along the reaction path as shown in Figure 2b. This kind of large variational effect has been observed for many reactions in the past.[16,36−42]

The sum of states $N_{k=1}(E,s)$ along the reaction path was calculated in order to obtain the rate constant by microcanonical[43,44] variational transition state theory. The sums of state $N_{k=1}(E,s)$ are plotted in Figure 3 for energies in the range

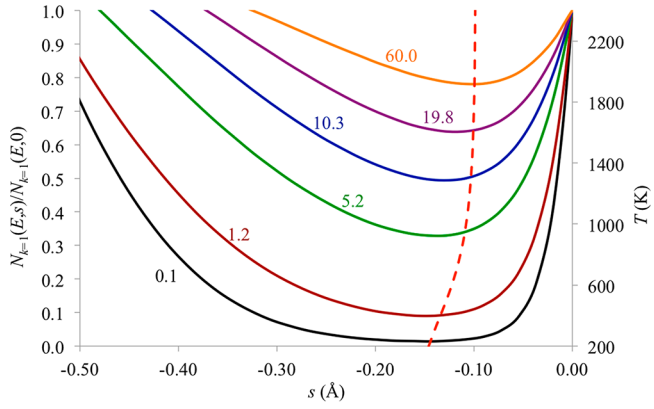

Figure 3. The sum of states $N_{k=1}(E,s)$, normalized by its value at the conventional transition state. The curves are labeled by total energy E in kcal/mol relative to the threshold energy. The red dashed line is the location of canonical variational transition state at various temperatures.

[0.1, 60] kcal/mol, and their values are normalized by $N_{k=1}(E,s=0)$. We also plot the location of the canonical variational transition state for temperatures from 200 to 2400 K. The minimum of each curve is the location of a microcanonical transition state at a given energy E. Figure 3 shows that the locations of the canonical variational transition states as functions of temperature are very close to the minima of the microcanonical curves. But the sums of states at the microcanonical variational transition states are all very different from those at the conventional transition state, and also the variational effects vary with energy. For example, at $E = 0.1$ kcal/mol, $N_{k=1}^{\mu VT}(E)$ is about 50 times smaller than $N_{k=1}(E, s=0)$, and at $E = 5.2$ kcal/mol, $N_{k=1}^{\mu VT}(E)$ is about 3 times smaller than $N_{k=1}(E,s=0)$. Conventional transition state theory is often used in the master equation solvers.[45−47] However, the present calculations show that if the sum of states at the conventional transition state is used to calculate energy-resolved rate constants, which are the quantities used in master equation treatments, the errors introduced by ignoring the variational effects could change the interpretation of experiments even qualitatively.

The reaction rate constants are calculated under the assumption that the system is in the low-pressure plateau region where the pressure is low enough for isolated binary collisions to be the reaction mechanism and there are no collision-stabilized pretransition-state complexes[48] (that could cause the rate

dx.doi.org/10.1021/ct400231q | J. Chem. Theory Comput. XXXX, XXX, XXX−XXX

constant to be pressure dependent—see the Appendix for further discussion of pressure dependence) but high enough that reactant states are in local equilibrium with each other during the reaction. Since the barrier of this reaction is negative (smaller than energy of reactant), there is no tunneling (we ignore nonclassical reflection here) for this reaction path in this plateau regime, so we set the tunneling transmission coefficients equal to unity and drop "/MT" in the rate expressions. Note, however, that other reaction paths (through the higher-energy transition structures) have tunneling contributions from energy levels above the energy of the reactant, but these tunneling contributions are associated with smaller Boltzmann factors and are ignored in the present study. The rate constants of this negative-barrier reaction in the low-pressure limit and high-pressure limit could have a factor 2 or less difference for temperatures between 300 and 200 K, but the difference would be expected to be negligible at temperatures above 500 K. These differences are caused by tunneling contributions from energy levels below the energy of reactants that are ignored in the low-pressure limit (see Appendix).

The calculated MS-TST, MS-CVT, and MS-μVT rate constant are listed in Table 2. The MS-TST rate constant is calculated with

Table 2. Rate Constants (cm^3 $molecule^{-1}$ s^{-1}) of R1

T (K)	MS-TST	MS−CVT	MS−μVT
200	3.04×10^{-12}	3.65×10^{-13}	3.61×10^{-13}
250	2.03×10^{-12}	3.96×10^{-13}	3.93×10^{-13}
298	1.67×10^{-12}	4.43×10^{-13}	4.39×10^{-13}
350	1.50×10^{-12}	5.06×10^{-13}	5.02×10^{-13}
400	1.44×10^{-12}	5.79×10^{-13}	5.75×10^{-13}
500	1.49×10^{-12}	7.53×10^{-13}	7.51×10^{-13}
600	1.66×10^{-12}	9.67×10^{-13}	9.65×10^{-13}
700	1.91×10^{-12}	1.22×10^{-12}	1.22×10^{-12}
800	2.22×10^{-12}	1.51×10^{-12}	1.51×10^{-12}
900	2.61×10^{-12}	1.85×10^{-12}	1.85×10^{-12}
1000	3.05×10^{-12}	2.24×10^{-12}	2.24×10^{-12}
1100	3.56×10^{-12}	2.67×10^{-12}	2.67×10^{-12}
1200	4.13×10^{-12}	3.16×10^{-12}	3.16×10^{-12}
1300	4.77×10^{-12}	3.69×10^{-12}	3.69×10^{-12}
1400	5.46×10^{-12}	4.29×10^{-12}	4.29×10^{-12}
1500	6.24×10^{-12}	4.94×10^{-12}	4.94×10^{-12}
1800	9.01×10^{-12}	7.24×10^{-12}	7.25×10^{-12}
2000	1.12×10^{-11}	9.09×10^{-12}	9.10×10^{-12}
2400	1.66×10^{-11}	1.36×10^{-11}	1.36×10^{-11}

$\gamma = 1$ in eq 1. The multistructural effect of the transition state, Y^{MS}, increases monotonically from 6.6 at 200 K to 17.3 at 2400 K. The reaction path was calculated by straight direct dynamics with energy, gradients, and Hessian calculated on the fly by the *GAUSSRATE* program.[35]

The key innovation in Table 2 is that the variation of torsional anharmonicity along a reaction path is included in the rate calculations. The MS-CVT and MS-μVT rates are quite lower than MS-TST rates due to the large variational effect shown in Figures 1 and 3. The calculated rate constants are not compared with experimental data in this letter, which is concerned with methodological issues. To compare to experimental results, we must calculate the rate constants of all the hydrogen abstraction channels; this will be done in a follow-up paper.

In this letter, torsional anharmonicity is shown to be critical for determining the location of the canonical and variational transition states and for rate constant calculations. The harmonic-oscillator approximation can lead to large errors in free energy profile calculations due to the variation of small frequencies along the reaction path. The torsional anharmonicity approximation of the MS-T method can treat this physical effect without significantly raising the computational cost of expensive reaction path calculations. Another simple treatment for the lowest frequency is replacing the HO approximation by using a free-rotor approximation for medium and high temperatures. To use the free-rotor partition function, one needs to assign the free-rotor mode to a particular uncoupled torsion and calculate its uncoupled moment of inertia. However, as is often true for both molecules and transition states, it is difficult to assign an uncoupled torsion to the lowest-frequency mode for the present reaction, and one cannot calculate an uncoupled reduced moment of inertia without the mode assignment. As we pointed out previously,[49] the product of uncoupled moments of inertia can be quite different from the product of coupled moments of inertia (determinant of $\mathbf{D}_j$). For example, the determinant of $\mathbf{D}_j$ could be a factor between 8 and 1.5 smaller than the product of uncoupled moments of inertia for the transition structures studied here.

APPENDIX: STEADY-STATE APPROXIMATION FOR PRESSURE EFFECT ON A BIMOLECULAR REACTION

Consider a bimolecular reaction A + B with a mechanism as shown in Figure A1, where C is a thermalized complex with

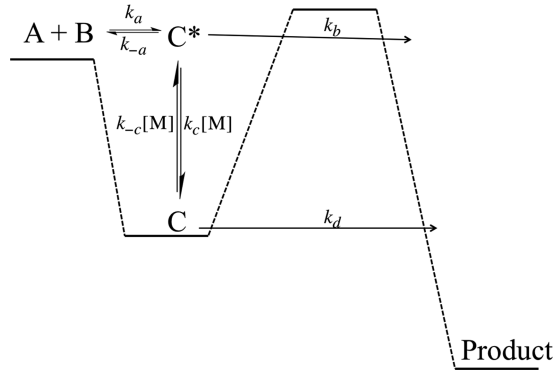

Figure A1. A mechanism for a bimolecular reaction A + B. The horizontal lines denote the ground-state energy levels of reactant, complex, transition state, and product, and [M] is the concentration of the third bodies (e.g., an inert gas diluent).

energy less than the reactant ground-state energy E_0^R, and C* is an activated complex with energy greater than or equal to E_0^R. The rate equations describing the time evolution of the concentrations are

$$\frac{d[A]}{dt} = -k_a[A][B] + k_{-a}[C^*] \quad \text{(A1)}$$

$$\frac{d[C^*]}{dt} = k_a[A][B] - k_{-a}[C^*] - k_c[M][C^*] + k_{-c}[M][C] - k_b[C^*] \quad \text{(A2)}$$

$$\frac{d[C]}{dt} = k_c[M][C^*] - k_{-c}[M][C] - k_b[C] \quad \text{(A3)}$$

where k_a, k_{-a}, k_c, k_{-c}, k_b, and k_d are rate constants for each elementary step. Note that k_d is nonzero only due to tunneling.

dx.doi.org/10.1021/ct400231q | J. Chem. Theory Comput. XXXX, XXX, XXX−XXX

The phenomenological rate k of the reaction A + B can be written as

$$\frac{d[\mathrm{A}]}{dt} = -k[\mathrm{A}][\mathrm{B}] \tag{A4}$$

Applying the steady state approximation for the concentrations of thermalized C and energized C*, we obtain the phenomenological rate constant as[50]

$$k = k_a\left\{1 - k_{-a}\left(k_{-a} + k_b + \frac{k_d k_c[\mathrm{M}]}{k_{-c}[\mathrm{M}] + k_d}\right)^{-1}\right\} \tag{A5}$$

If tunneling is ignored in eq A5 (i.e., if k_d is zero), or if we are in the low-pressure limit, the rate k becomes[50]

$$k^{\mathrm{low}[M]} = k_b\left\{\frac{k_a}{k_{-a} + k_b}\right\} \tag{A6}$$

This is independent of pressure, and if $k_b \ll k_{-a}$, it is the same as the rate constant calculated by transition state theory without considering the intermediate C and without considering the tunneling contribution from energy levels below energy of reactants.

AUTHOR INFORMATION

Corresponding Author

*E-mail: truhlar@umn.edu.

Notes

The authors declare no competing financial interest.

ACKNOWLEDGMENTS

This work was supported in part by the U.S. Department of Energy, Office of Science, Office of Basic Energy Sciences, under grant no. DE-FG02-86ER13579, and as part of the Combustion Energy Frontier Research Center under award number DE-SC0001198.

REFERENCES

(1) Wigner, E. *J. Chem. Phys.* **1937**, *5*, 720−725.
(2) Horiuti, J. *Bull. Chem. Soc. Jpn.* **1938**, *13*, 210−216.
(3) Keck, J. C. *J. Chem. Phys.* **1960**, *32*, 1035−1050.
(4) Garrett, B. C.; Truhlar, D. G. *J. Chem. Phys.* **1979**, *70*, 1593−1598.
(5) Pechukas, P. *Annu. Rev. Phys. Chem.* **1981**, *32*, 159−177.
(6) Truhlar, D. G.; Garrett, B. C. *Annu. Rev. Phys. Chem.* **1984**, *35*, 159−189.
(7) Truhlar, D. G.; Garrett, B. C.; Klippenstein, S. J. *J. Phys. Chem.* **1996**, *100*, 12771−12800.
(8) Fernández-Ramos, A.; Miller, J. A.; Klippenstein, S. J.; Truhlar, D. G. *Chem. Rev.* **2006**, *106*, 4518−4584.
(9) Isaacson, A. D.; Truhlar, D. G. *J. Chem. Phys.* **1982**, *76*, 1380−1391.
(10) Jackels, C. F.; Gu, Z.; Truhlar, D. G. *J. Chem. Phys.* **1995**, *102*, 3188−3201.
(11) Truhlar, D. G.; Kuppermann, A. *J. Am. Chem. Soc.* **1971**, *93*, 1840−1851.
(12) Alecu, I. M.; Zheng, J.; Zhao, Y.; Truhlar, D. G. *J. Chem. Theory Comput.* **2010**, *6*, 2872−2887.
(13) Zheng, J.; Yu, T.; Papajak, E.; Alecu, I. M.; Mielke, S. L.; Truhlar, D. G. *Phys. Chem. Chem. Phys.* **2011**, *13*, 10885−10907.
(14) Zheng, J.; Truhlar, D. G. *J. Chem. Theory Comput.* **2013**, *9*, 1356−1367.
(15) Yu, T.; Zheng, J.; Truhlar, D. G. *J. Phys. Chem. A* **2012**, *116*, 297−308.
(16) Zheng, J.; Truhlar, D. G. *Faraday Discuss.* **2012**, *157*, 59−88.
(17) Yu, T.; Zheng, J.; Truhlar, D. G. *Chem. Sci.* **2011**, *2*, 2199−2213.
(18) Garrett, B. C.; Truhlar, D. G. *J. Am. Chem. Soc.* **1979**, *101*, 4534−4548.
(19) Kilpatrick, J. E.; Pitzer, K. S. *J. Chem. Phys.* **1949**, *17*, 1064−1075.
(20) Zheng, J.; Mielke, S. L.; Clarkson, K. L.; Truhlar, D. G. *Comput. Phys. Commun.* **2012**, *183*, 1803−1812.
(21) Zheng, J.; Mielke, S. L.; Clarkson, K. L.; Truhlar, D. G. *MSTor*, version 2013; University of Minnesota: Minneapolis, MN, 2013.
(22) Zheng, J.; Meana-Pañeda, R.; Truhlar, D. G. *Comput. Phys. Commun.* **2013**, *184*, 2032−2033.
(23) Forst, W. *Unimolecular Reactions − A Concise Introduction*; Cambridge University Press: Cambridge, U. K., 2003; p 78.
(24) Peslherbe, G. H.; Hase, W. L. *J. Chem. Phys.* **1996**, *104*, 9445−9460.
(25) Jackels, C. F.; Gu, Z.; Truhlar, D. G. *J. Chem. Phys.* **1995**, *102*, 3188−3201.
(26) Nguyen, K. A.; Jackels, C. F.; Truhlar, D. G. *J. Chem. Phys.* **1996**, *104*, 6491−6496.
(27) Zhao, Y.; Truhlar, D. G. *J. Chem. Theory Comput.* **2008**, *4*, 1849−1868.
(28) Clark, T.; Chandrasekhar, J.; Spitznagel, G. W.; Schleyer, P. v. R. *J. Comput. Chem.* **1983**, *4*, 294−301.
(29) Lynch, B. J.; Zhao, Y.; Truhlar, D. G. *J. Phys. Chem. A* **2003**, *107*, 1384−1388.
(30) Raghavachari, K.; Trucks, G. W.; Pople, J. A.; Head-Gordon, M. *Chem. Phys. Lett.* **1989**, *157*, 479−483.
(31) Adler, T. B.; Knizia, G.; Werner, H.-J. *J. Chem. Phys.* **2007**, *127*, 221106/1−4.
(32) Knizia, G.; Adler, T. B.; Werner, H.-J. *J. Chem. Phys.* **2009**, *130*, 054104/1−20.
(33) Papajak, E.; Truhlar, D. G. *J. Chem. Theory Comput.* **2010**, *6*, 597−601.
(34) Zheng, J.; Zhang, S.; Lynch, B. J.; Corchado, J. C.; Chuang, Y.-Y.; Fast, P. L.; Hu, W.-P.; Liu, Y.-P.; Lynch, G. C.; Nguyen, K. A.; Jackels, C. F.; Ramos, A. F.; Ellingson, B. A.; Melissas, V. S.; Villà, J.; Rossi, I.; Coitino, E. L.; Pu, J.; Albu, T. V.; Steckler, R.; Garrett, B. C.; Isaacson, A. D.; Truhlar, D. G. *POLYRATE*; University of Minnesota: Minneapolis, MN, 2012; locally modified version based on version 2010-A.
(35) Zheng, J.; Zhang, S.; Corchado, J. C.; Chuang, Y.-Y.; Coitiño, E. L.; Ellingson, B. A.; Truhlar, D. G. *GAUSSRATE*; University of Minnesota, Minneapolis, MN, 2010; locally modified version based on version 2009-A.
(36) Truhlar, D. G.; Garrett, B. C. *Acc. Chem. Res.* **1980**, *13*, 440−448.
(37) Garrett, B. C.; Truhlar, D. G. *J. Am. Chem. Soc.* **1979**, *101*, 4534−4548.
(38) Garrett, B. C.; Truhlar, D. G.; Grev, R. S.; Magnuson, A. W. *J. Phys. Chem.* **1980**, *84*, 1730−1748; Erratum: **1983**, *87*, 4554.
(39) Garrett, B. C.; Truhlar, D. G. *J. Am. Chem. Soc.* **1980**, *102*, 2559−2570.
(40) Truhlar, D. G.; Isaacson, A. D.; Skodje, R. T.; Garrett, B. C. *J. Phys. Chem.* **1982**, *86*, 2252−2261.
(41) Garrett, B. C.; Truhlar, D. G.; Wagner, A. F.; Dunning, T. H. *J. Chem. Phys.* **1983**, *78*, 4400−4413.
(42) Zheng, J. J.; Rocha, R. J.; Pelegrini, M.; Ferrão, L. F. A.; Carvalho, E. F. V.; Roberto-Neto, O.; Machado, F. B. C.; Truhlar, D. G. *J. Chem. Phys.* **2012**, *136*, 184310/1−10.
(43) Garrett, B. C.; Truhlar, D. G *J. Phys. Chem.* **1979**, *83*, 1079−1112.
(44) Isaacson, A. D.; Sund, M. T.; Rai, S. N.; Truhlar, D. G. *J. Chem. Phys.* **1985**, *82*, 1338−1340.
(45) Fernández-Ramos, A.; Miller, J. A.; Klippenstein, S. J.; Truhlar, D. G. *Chem. Rev.* **2006**, *106*, 4518−4584.
(46) Barker, J. R. *Int. J. Chem. Kinet.* **2009**, *41*, 748−763.
(47) Glowacki, D. R.; Liang, C.-H.; Morley, C.; Pilling, M. J.; Robertson, S. H. *J. Phys. Chem. A* **2012**, *116*, 9545−9560.
(48) (a) Benson, S. W.; Dobis, O. *J. Phys. Chem. A* **1998**, *102*, 5175−5181. (b) Alecu, I. M.; Gao, Y.; Hsieh, P.-C.; Sand, J. P.; Ors, A.; McLeod, A.; Marshall, P. *J. Phys. Chem. A* **2007**, *111*, 3970−3976. (c) Greenwald, E. E.; North, S. M.; Georgievskii, Y.; Klippenstein, S. J. *J. Phys. Chem. A* **2005**, *109*, 6031−6044.

(49) Alecu, I. M.; Zheng, J.; Papajak, E.; Yu, T.; Truhlar, D. G. *J. Phys. Chem. A* **2012**, *116*, 12206−12213.
(50) Brown, S. S.; Burkholder, J. B.; Talukdar, R. K.; Ravishankara, A. R. *J. Phys. Chem. A* **2001**, *105*, 1605−1614.